Uncooled Multimirror Broad-Band Infrared Microbolometers

Mahmoud Almasri, *Student Member, IEEE*, Zeynep Çelik-Butler, *Senior Member, IEEE*, Donald P. Butler, *Senior Member, IEEE*, Alparslan Yaradanakul, *Student Member, IEEE*, and Ali Yildiz

***Abstract*—A new generation of microbolometers were designed, fabricated and tested for the NASA CERES (Clouds and the Earth's Radiant Energy System) instrument to measure the radiation flux at the Earth's surface and the radiant energy flow within the atmosphere. These detectors are designed to measure the earth radiances in three spectral channels consisting of a short wave channel of 0.3 to 5 μm, a wide-band channel of 0.3 to 100 μm and a window channel from 8 to 12 μm each housing a 1.5 mm $\times$ 1.5 mm microbolometers or alternatively 400 μm $\times$ 400 μm microbolometers in a 1 $\times$ 4 array of detectors in each of the three wavelength bands, thus yielding a total of 12 channels. The microbolometers were fabricated by radio frequency (RF) magnetron sputtering at ambient temperature, using polyimide sacrificial layers and standard micromachining techniques. A semiconducting YBaCuO thermometer was employed. A double micromirror structure with multiple resonance cavities was designed to achieve a relatively uniform absorption from 0.3 to 100 μm wavelength. Surface micromachining techniques in conjunction with a polyimide sacrificial layer were utilized to create a gap underneath the detector and the Si_3N_4 bridge layer. The temperature coefficient of resistance was measured to be -2.8%/K. The voltage responsivities were over 10^3 V/W, detectivities above 10^8 cm Hz$^{1/2}$/W, noise equivalent power less than 4×10^{-10} W/Hz$^{1/2}$ and thermal time constant less than 15 ms. [759]**

***Index Terms*—Broadband, detection, far infrared, infrared, microbolometer, uncooled, yttrium barium copper oxide.**

I. Introduction

In THE last few years, uncooled infrared (IR) detection systems have shown considerable progress in cost, size, and performance, both for military and commercial applications. In transportation, IR cameras are used to improve the driver's ability to see in darkness. In rescue operations, they allow firefighters to distinguish victims through the smoke. In earth science research, IR vision systems are used to measure physical properties of cloud radiation [1], [2]. Microbolometer technology is employed in this paper because it can operate at room temperature and it possesses a relatively flat broadband spectral response. Microbolometric devices exhibit a change in resistance with respect to a change of temperature of the sensing material accompanying the absorption of infrared radiation [3].

In our previous works, several different designs of semiconducting YBaCuO microbolometers were reported, utilizing: SiO_2 bridges bulk-Si-micromachined to hold the detector arrays; Si_3N_4 membranes surface-micromachined using a MgO sacrificial layer; and surface micromachined YBaCuO detectors, self-supported by thin titanium electrode arms [4]–[10].

The most commonly used infrared detectors are based on the photovoltaic effect such as HgCdTe detectors, which have achieved detectivity of $(1 - 3) \times 10^{10}$ cm Hz$^{1/2}$/W in long-wavelength infrared applications when cooled to 77 K [11], [12]. However these detectors are limited by their narrow spectral bandwidth response and fail to reach to far IR region. On the other hand, broadband spectral response can be achieved easily using thermal detectors. Uncooled thermopile detectors are commonly used for radiometric applications. A specifically designed thermopile detector with an area of 200 $\times$ 200 μm^2 operating between 2.5–50 μm region of the far IR spectrum has been reported to show responsivity around 400 V/W, detectivity of 1.7×10^8 cm Hz$^{1/2}$/W with a response time of 37 ms [13]. In addition, square grid metalized silicon nitride bolometers have been used for far IR detection. These suspended micromesh bolometers have achieved noise equivalent power (NEP) as low as 2.7×10^{-17} W/Hz$^{1/2}$ at 304 mK with a response time of 24 ms [14]. Other types of far-IR thermal detectors are the conventional high-T_c superconducting transition edge bolometers [15]–[18], and antenna-coupled superconducting microbolometers [19], [20]. High-T_c superconducting $YBa_2Cu_3O_x$ detectors have exhibited responsivity as high as 1.7×10^4 V/W and NEP as low as 2.1×10^{-14} W/Hz$^{1/2}$ [21]. Similarly, superconducting $YBa_2Cu_3O_{7-x}$ microbolometers with bowtie antennas on $NdGaO_3$ have achieved NEP as low as 1.2×10^{-12} W/Hz$^{1/2}$ and thermal response time of 20 ns [19]. Antenna-coupled superconducting microbolometers have a faster response time and a comparable NEP to that of conventional superconducting microbolometers. However, the high cost of cooling, and the requirement for high deposition temperatures limit the application of high-T_c superconductor bolometers.

In this paper, novel semiconducting YBaCuO microbolometers are developed for far-infrared wavelength detection. The key feature of the structures is that the detector arrays are smaller and faster than those currently used in CERES, while retaining the requirement for spectral flatness of the total detector system. In addition, the sensitivity of the detectors is improved by an order of magnitude compared to the currently used IR detectors.

Manuscript received September 19, 2001; revised March 18, 2002. This work was supported in part by NASA (NAS1-99100), the National Science Foundation (ECS-9800062), and Army Research Office (38673PH). Subject Editor G. B. Hocker.

M. Almasri and A. Yaradanakul are with the Department of Electrical Engineering, Southern Methodist University, Dallas, TX 75275-0338 USA.

Z. Çelik-Butler and D. P. Butler were with the Department of Electrical Engineering, Southern Methodist University, Dallas, TX 75275-0338 USA. They are now with the Department of Electrical Engineering, University of Texas at Arlinton, Arlington, TX 76109 USA (e-mail: zbutler@uta.edu; dbutler@uta.edu).

Digital Object Identifier 10.1109/JMEMS.2002.803413.

These microbolometers are fabricated with a polyimide sacrificial layer and sputtered thin films. Detectors are designed with two different areas. The first type of detector utilizes a single 1.5×1.5 mm^2 bolometer while the second type is a 1×4-detector array made of 0.4×0.4 mm^2 bolometers fitting into the footprint of the present single detectors. The purpose of this research is to replace the existing technology, thus allowing a new generation of CERES instruments to measure the radiation flux at the Earth's surface and the radiant energy flow within the atmosphere.

Several figures of merits are used to characterize the microbolometric devices such as responsivity, R_V, detectivity, D^*, and temperature coefficient of resistance *(TCR)*. Responsivity is the amount of output seen per watt of input radiant optical power.

$$R_V = \frac{I_b R \beta \eta}{G(1+\omega^2 \tau_{th}^2)^{1/2}} \tag{1}$$

where I_b is the bias current, R is the dc resistance, η is the absorptivity, G is the total thermal conductance to the substrate, ω is the radiation modulation frequency, τ_{th} is the thermal response time, defined by the ratio of the device thermal mass to its thermal conductance, and β is the thermal coefficient of resistance (TCR) given by $(1/R)(dR/dT)$.

The detectivity measures the signal-to-noise ratio (SNR) normalized with respect to the detector active area

$$D^* = \frac{R_V \sqrt{\Delta f \ A}}{\Delta V_n}. \tag{2}$$

Here, Δf is the amplifier frequency bandwidth. The noise voltage, ΔV_n, includes the background noise, the temperature fluctuation noise, and the noise generated by the thermometer, which is made up of Johnson noise and $1/f$-noise.

An important figure of merit for a detector is its noise equivalent power (NEP), the input power necessary to give a signal-to-noise ratio of unity [3], [22]:

$$NEP = \frac{\Delta V_n}{R_v}. \tag{3}$$

Hence, for good performance, a microbolometer must have large values of β, R_V, D^* and low *NEP*.

II. Microbolometer Design

A 3-D view of the 400×400 μm^2 microbolometer is shown in Fig. 1. In this design, a novel double-mirror structure is used underneath the pixel to achieve a flat spectral response. One mirror is roughly tuned toward absorption at longer wavelengths with a cavity height of 3.68 μm, while the second mirror is tuned toward mid wavelengths with a cavity height of approximately 2.73 μm. A transmission line model was used to match the impedance of the detector thin film layers to free space impedance, 377 Ω, by adjusting the height of the two microcavities between the suspended thermometer and the underlying mirrors and optimizing the thicknesses of the thin films forming the overall structure. An equal-area weighing was imposed as one of the constraints in the Monte Carlo and Gradient optimization techniques used for this purpose. The result was a flattened spectral response with an enhanced absorption. The net effect was to use two 1/4-wave resonances to minimize the fluctuation in the spectral response and achieve the desired broadband

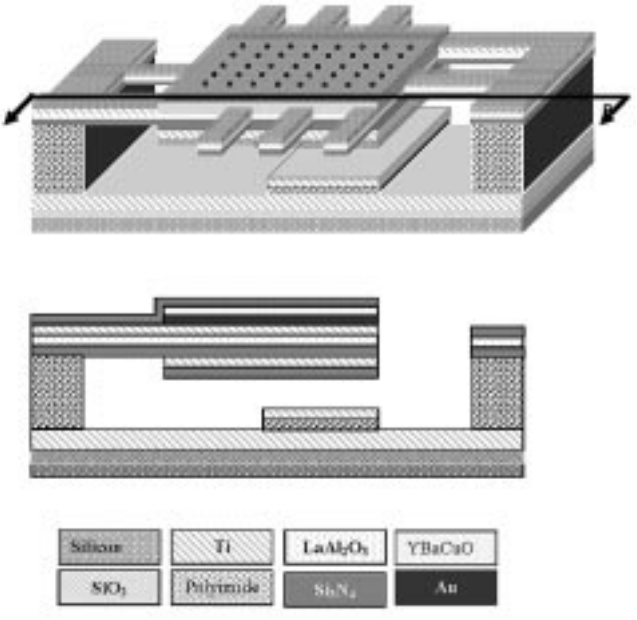

Fig. 1. A 3-D view of the 400×400 μm^2 microbolometer geometry. Above, a perspective schematic and below a cross-section showing the layers in the structure. The schematics show the device geometry consisting of double mirrors, double absorbers, Si_3N_4 membrane and passivation layer, and Ti electrode arms with Au contacts to the YBaCuO thermometer.

impedance match. The results of single and double microcavity design are plotted in Fig. 2. The YBaCuO thermometer and Si_3N_4 supporting membrane have a resonance, which is mixed with the resonance of the two microcavities. Therefore, a regular resonance pattern was not observed. A thin absorber layer was used to enhance the absorption at long wavelengths.

In this structure, a two-metal-electrode was employed. Au ($\kappa = 3.1$ W/cmK) was chosen since it makes a good electrical contact to YBaCuO. The Au contacts were designed with narrow and long rectangular shapes to provide uniform current throughout the pixel. Ti makes a higher resistance contact to YBaCuO but has a relatively low thermal conductivity ($\kappa =$ 0.219 W/cmK) and therefore provides a better thermal isolation than if a single, high thermal conductivity Au electrode was used.

III. Microbolometer Fabrication

YBaCuO microbolometers were fabricated in two different sizes using conventional polyimide sacrificial layers and a Si_3N_4 supporting membrane. The 400×400 μm^2 size microbolometers were fabricated in 1×4 arrays suspended above the substrate by a supporting membrane. The 1.5×1.5 mm^2 microbolometers were fabricated as a single pixel. Due to the need for relatively high thermal conductance to achieve low-time constant while maintaining the large detector size (and therefore large thermal capacitance), the supporting membranes were designed with shorter and wider supporting arms. Fig. 3 shows the SEM micrograph of the resulting devices. The detectors were processed at room temperature, except for the polyimide cure, using a combination of RF magnetron sputter deposition, surface micromachining and selective wet and plasma etching techniques.

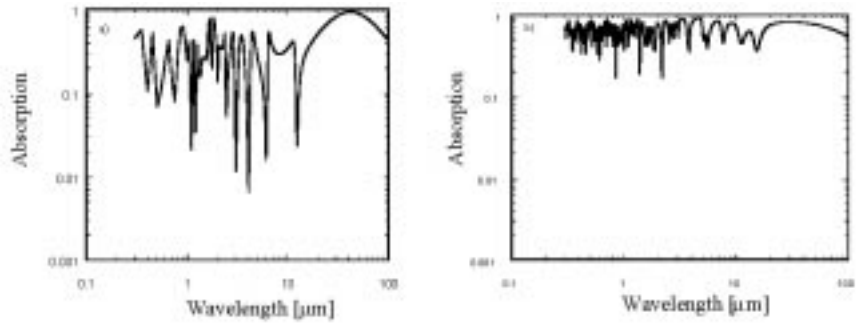

Fig. 2. Calculated absorption spectra for (a) one-mirror and (b) two-mirror microbolometer designs. The two-mirror design considerably flattens the spectral response of the microbolometer.

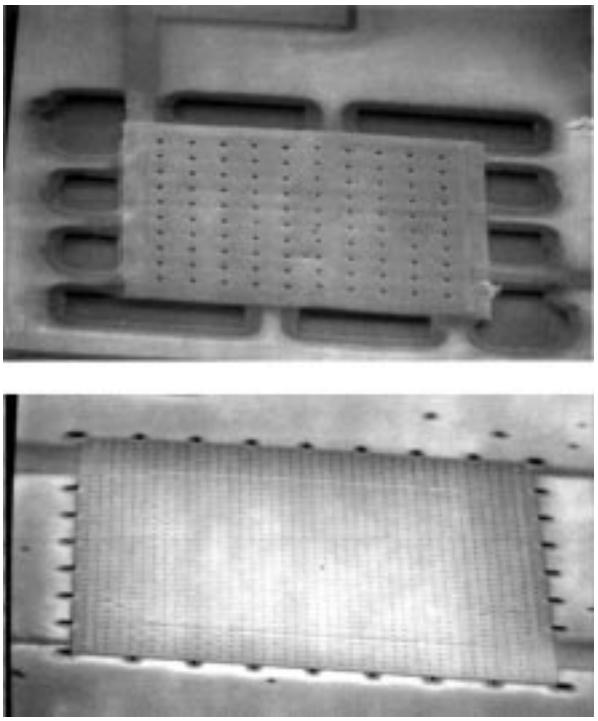

Fig. 3. An SEM micrograph of the resulting devices: 400 × 400 μm^2 pixel from a 1 × 4 array (top); a single 1.5 × 1.5 mm^2 pixel (bottom). The outline of the mirror underneath the cavity can be seen in the large area device.

The device fabrication steps are described as follows. Oxidized Si wafers were coated with a thick Ti mirror layer deposited by RF magnetron sputtering. The nominal thickness of Ti was 370 nm. The continuous titanium mirror reflects the IR radiation transmitted back to the active pixel area, forming a resonant cavity with YBaCuO thermometer to enhance the IR absorption. In addition, it prevents the excitation of the electron–hole pairs in the substrate. The wafers were then spin coated with Dupont polyimide (PI2611) and soft baked. The polyimide was then cured at 270 °C in N_2 environment for 1 hour to obtain a durable film, nominally 2.33 μm thick. This represents the highest processing temperature in the fabrication. Next, the second 300-nm thick Ti mirror was similarly deposited by RF magnetron sputtering and patterned with standard photolithographic techniques. The areas of the two mirrors forming the two microcavities were set to be equal. The second polyimide sacrificial layer was again spin-coated and cured to the nominal thickness of 3.68 μm. Next, a 13 nm thick Si_3N_4 passivation layer was deposited followed by sputtering of a thin (4 nm) titanium absorber. The passivation and absorber layers were then defined with an area equal to the pixel size. A 236 nm thick Si_3N_4 membrane material was subsequently deposited, followed by 23 nm of $LaAl_2O_3$. This layer is used as an etch stop to protect Si_3N_4 during plasma etching of Ti electrode arms.

The metallization layers were formed consisting of Ti electrode arms (120 nm) and Au contacts/pads (100 nm). Gold was patterned and wet etched. Then, titanium layer was patterned and plasma etched. Next, 350 nm of semiconducting YBaCuO thermometer layer was deposited by RF magnetron sputtering at ambient temperature from a single, commercially available $YBa_2Cu_3O_{6+x}$ sputter target. The YBaCuO pixel was patterned using standard photolithographic and wet etching techniques. Trench cuts were then patterned and etched through the $LaAl_2O_3$ and Si_3N_4 layers to expose the polyimide to oxygen ashing in the final step. Access holes with dimensions of 3 × 3 μm^2 and 4 × 4 μm^2 were patterned on top of YBaCuO. These holes are necessary to allow access to the sacrificial layer underneath the pixel and to fully release such large size microbolometers. Both YBaCuO and $LaAl_2O_3$ were wet etched in the same solution. Using the photoresist mask, the holes through supporting Si_3N_4 membrane, the Ti-absorber and the passivation Si_3N_4 were dry etched in $Ar:CF_4$. The trench cuts and holes were realigned, patterned and wet-etched. Subsequently, the bonding contacts were patterned and dry etched.

Finally, oxygen plasma ashing was done to remove the polyimide layer suspending the YBaCuO pixel and forming the thermal isolation structure. The YBaCuO thermometer was protected during this step with a passivation layer of Si_3N_4 atop YBaCuO. The undercut procedure was interrupted every 30 min to allow cooling of the structure thus minimizing stress-cracking.

IV. Results and Discussion

Microbolometers were mounted in a Leybold ROK 10–300 K closed-cycle refrigerator, evacuated to 50 mtorr. Both 400 × 400 μm^2 1 × 4 arrays and 1.5 × 1.5 mm^2 single pixels were characterized. The two-probe resistance for most of the devices ranged from 1.5 – 5 MΩ, depending on the geometry, with linear I–V characteristics up to 7 μA with no evidence of joule heating. The TCR was measured in 240–320 K temperature range to be

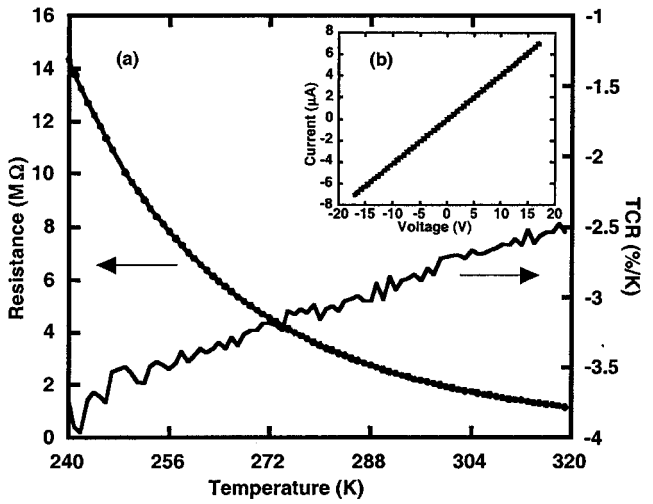

Fig. 4. Resistance and temperature coefficient of resistance as a function of temperature over the temperature range of 240 to 320 K for a 400 × 400 μm^2 microbolometer. The inset displays the linear current–voltage characteristic of the device.

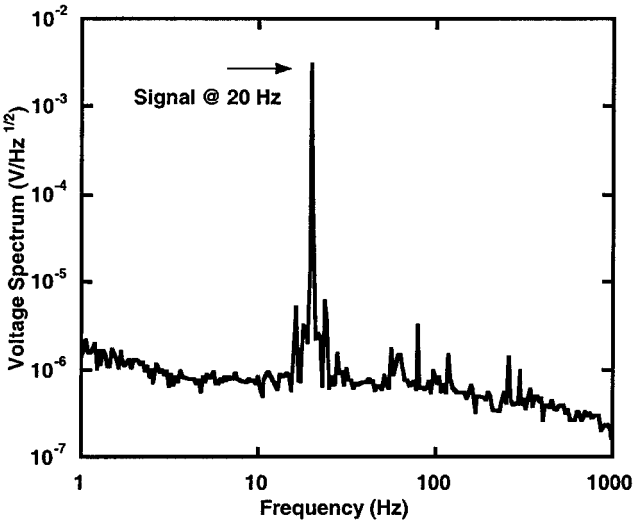

Fig. 5. Typical signal spectra from a 1.5 × 1.5 mm^2 microbolometer. The signal was measured with a current bias of 4.65 μA. The chopping frequency is 20 Hz.

2.88% K^{-1} and 2.74% K^{-1} for the 400 × 400 μm^2 and 1.5 × 1.5 mm^2 microbolometers, respectively. The measured resistance, the corresponding TCR versus temperature and I–V characteristics are shown in Fig. 4. These TCR values are lower in magnitude than what was previously reported for semiconducting YBaCuO, which were about 3.5%/K [6], [5]. The lower TCR value can be attributed to the exposure of YBaCuO thermometer to oxygen plasma during the ashing of the polyimide to form the suspended structure. The relative increase of oxygen concentration causes YBaCuO to exhibit lower resistivity and TCR because the Fermi energy gets closer to the mobility band edge for holes, thus decreasing the activation energy for conduction of majority carriers, holes in this case [23].

The thermal conductance of the pixel to the substrate was extracted through the Joule-heating method using resistance versus temperature characteristics measured with bias current up to 4 μA. G was 1.68 × 10^{-5}W/K and 5.7 × 10^{-5}W/K for small area and large area devices, respectively. The thermal conductance of the small area microbolometer was designed to be lower than the large area microbolometer to produce approximately the same thermal time constant. The smaller microbolometer has a correspondingly smaller thermal mass. An error in the estimation of the thermal conductivity of Si_3N_4 resulted in lower thermal conductances than planned in both cases, hence larger thermal time constants than intended.

The voltage responsivity and detectivity figures of merit were evaluated with a set of Oriel Instruments, consisting of a 1450 K mock-blackbody light source: 6575 IR ceramic element and 60 077 ZnSe condenser/collimator. The net usable wavelength range of this broadband system was ∼0.6–15 μm. The intensity of the optical power was 6.3 mW/cm^2 on the small area devices and 3.4 mW/cm^2 on the large area devices. The measurements were performed inside an electromagnetically shielded room. The devices were mounted inside a cryostat evacuated to 50 mtorr. The IR radiation was mechanically chopped through a ZnSe window. The microbolometers were dc biased with a current varying from 0.156 to 10 μA, supplied by a low noise, battery-powered current source. The voltage signal for each chopping frequency were amplified with a PAR-113 preamplifier and averaged with a Hewlett-Packard 3562 a dynamic signal analyzer. The responsivity R_v of the detectors was calibrated against an Oriel 70 124 calibrated detector. A typical voltage spectrum measured on a large area detector biased with 4.65 μA is shown in Fig. 5 in response to the broadband IR source chopped at 20 Hz.

The responsivity, and detectivity are plotted in Fig. 6, as a function of chopping frequency for two bias currents. The measured responsivity and detectivity of the 400 × 400 μm^2 size microbolometers reached up to 1.56 × 10^3 V/W and 1.25 × 10^8 cm Hz$^{1/2}$/W, respectively, at I_b = 4.65 μA. For the 1.5 × 1.5 mm^2 size microbolometers, the highest responsivity and detectivity were 158 V/W and 3.48 × 10^7 cm Hz$^{1/2}$/W at I_b = 4.28 μA. The noise equivalent power was measured to be as low as 3.21 × 10^{-10} W/Hz$^{1/2}$ for small area detectors and ∼4.3 × 10^{-9} W/Hz$^{1/2}$ for large area detectors at the same bias currents (see Fig. 7). The larger responsivity and lower NEP of the small area detectors is a consequence of the smaller thermal conductance G designed into these detectors. The power normalized $1/f$ noise corner frequency [10] was around 0.2–0.5 Hz/μW for 400 × 400 μm^2 devices and 1.1–1.8 Hz/μW for 1.5 × 1.5 mm^2 devices. This is considerably lower than the noise exhibited by VO_x [24] and a : Si microbolometers [25]. Comparisons for the detectivity figure of merit can be made to the temperature fluctuation noise limited and background noise limited detectivity [26]. Substituting the temperature fluctuation noise as the dominant noise voltage into (2), yields the temperature fluctuation noise limited detectivity to be

$$D^*_{TF} = \sqrt{\frac{\eta^2 A}{4kT_D^2 G}} \tag{4}$$

where T_D is the detector temperature. Similarly, substituting the background noise associated with the radiative exchange between the detector and its environment yields a detectivity given by

$$D^*_{BG} = \sqrt{\frac{\eta}{8k\left(T_D^5 + T_B^5\right)\sigma}} \tag{5}$$

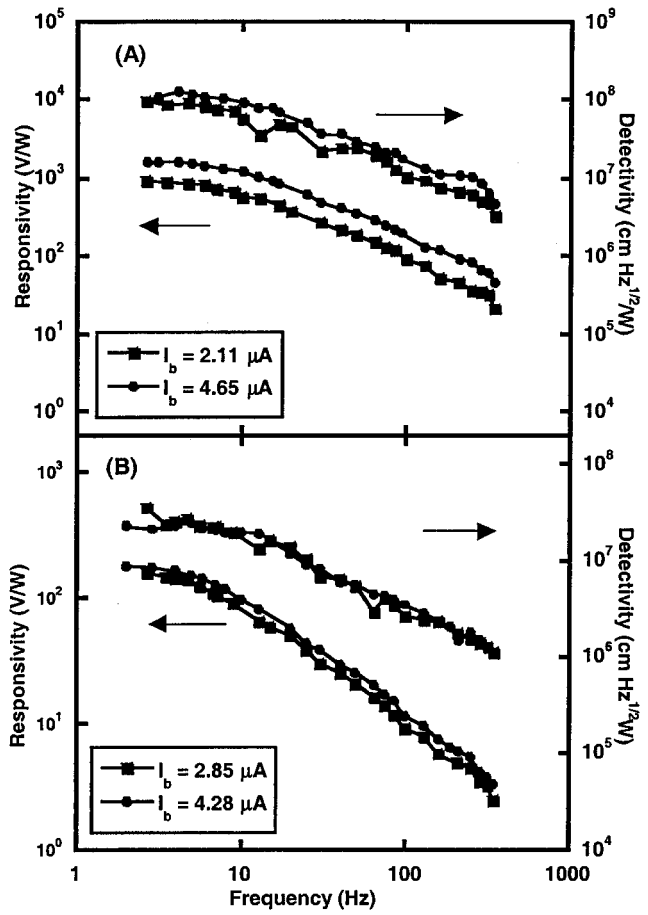

Fig. 6. Responsivity and detectivity as a function of chopper frequency at different current bias values measured in vacuum with 0.6 to 15 μm broadband IR radiation. (a) 400 μm $\times$ 400 μm size microbolometer and (b) 1.5 mm $\times$ 1.5 mm size microbolometer.

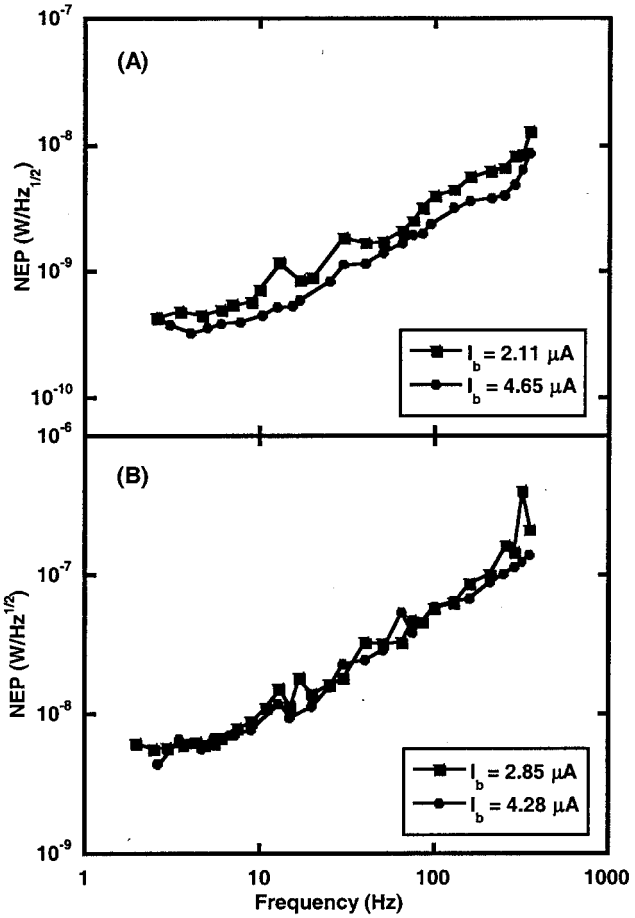

Fig. 7. Noise equivalent power as a function of chopper frequency (a) for 400 μm $\times$ 400 μm size microbolometer and (b) for the 1.5 mm $\times$ 1.5 mm size microbolometer. NEP was measured in vacuum with 0.6 to 15 μm broadband IR radiation at different current biases.

where T_B is the background or scene temperature and σ is the Stefan–Boltzmann constant. Using the measured parameters presented in Table I, the temperature fluctuation noise limited detectivity is calculated to be 2.6 $\times$ 10^9 cm $Hz^{1/2}$/W and 4.5 $\times$ 10^9 cm $Hz^{1/2}$/W for the small area 0.4 mm $\times$ 0.4 mm and large area 1.5 mm $\times$ 1.5 mm microbolometers respectively. Assuming the background temperature T_B is the temperature of the source, 1450 K, and the detector temperature is 300 K, the background noise limited detectivity is calculated to be approximately 4 $\times$ 10^8 cm $Hz^{1/2}$/W for both detectors. The measured detectivity is less than both these limits implying that further reduction in the thermal conductivity G is necessary to obtain higher detectivity. However the thermal mass and desired thermal time constant limit the achievable reduction.

The spectral response was measured in vacuum as a function of IR wavelength over the range from 0.6 to 15 μm with an Oriel monochromator, and the same blackbody source. The spectral response versus wavelength figure displays mixed absorption resonance, which is composed of the resonance of the relatively thick layers of YBaCuO and Si_3N_4 and the two cavities. The measured spectral response was relatively flat with at most an order of magnitude variation over the measured wavelength band (see Fig. 8). The decrease of responsivity in the 4 to 8 μm band is mainly due to the lower than expected absorption of the Ti absorber in this band. The transmission line model (see Fig. 2) predicts approximately a factor of four variation in the absorption over this wavelength range. The difference between the predicted absorption and the measured one is most likely due to the partial oxidation of Ti absorber that resulted from the exposure to oxygen during plasma ashing of the polyimide layer to suspend the structure. It might also be due to the slight variation between the fabricated and the calculated thin film thicknesses. The absorption can be further enhanced to provide a flatter spectral response by further optimization of the device structure by adding another resonance or perhaps introducing an on-chip antenna. Improvement in the microbolometer responsivity, detectivity and noise equivalent power requires a decreased thermal mass to shorten the thermal time constant and a reduction in the thermal conductance.

The NEP was also measured as a function of IR wavelength and is displayed in Fig. 9. The relatively high values observed in 4–8 μm range is believed to be due to the low signal (see Fig. 8) in this range and therefore an artifact introduced from the measurement setup noise.

The thermal time constants, $\tau_{\rm th}$ were calculated using the responsivity vs. chopper frequency data in conjunction with (1). $\tau_{\rm th}$ ranged from 13 to 15 ms for the small area devices and from 25 to 28 ms for the large area devices. The extrapolated thermal

TABLE I
SUMMARY OF THE RESULTS FOR 400 μm × 400 μm 1 × 4 ARRAYS AND 1.5 mm × 1.5 mm SINGLE PIXEL DETECTORS

Device area	400×400 μm^2	1.5 × 1.5 mm^2
2-Wire resistance at 295 K (MΩ)	2.42	2.0
TCR (%/K)	2.88	2.74
Thermal conductance G (W/K)	1.68×10^{-5}	5.7×10^{-5}
Thermal capacitance C (J/K)	2.52×10^{-7}	1.47×10^{-6}
Thermal time constant τ_{th}(ms)	15	25.8
Maximum responsivity R_v (V/W)	1.56×10^{3} @ 4.65 μA	157.7 @ 4.28 μA
Maximum detectivity D^* (cm $Hz^{1/2}$/W)	1.25×10^{8} @ 4.65 μA	3.48×10^{7} @ 4.28μA
NEP (W/$Hz^{1/2}$)	3.21×10^{-10} @ 4.65 μA	4.3×10^{-9} @ 4.28 μA
Power normalized 1/f noise corner frequency f_c Hz/μW	0.2 – 0.5	1.1 – 1.8
Absorption (%)	60	50

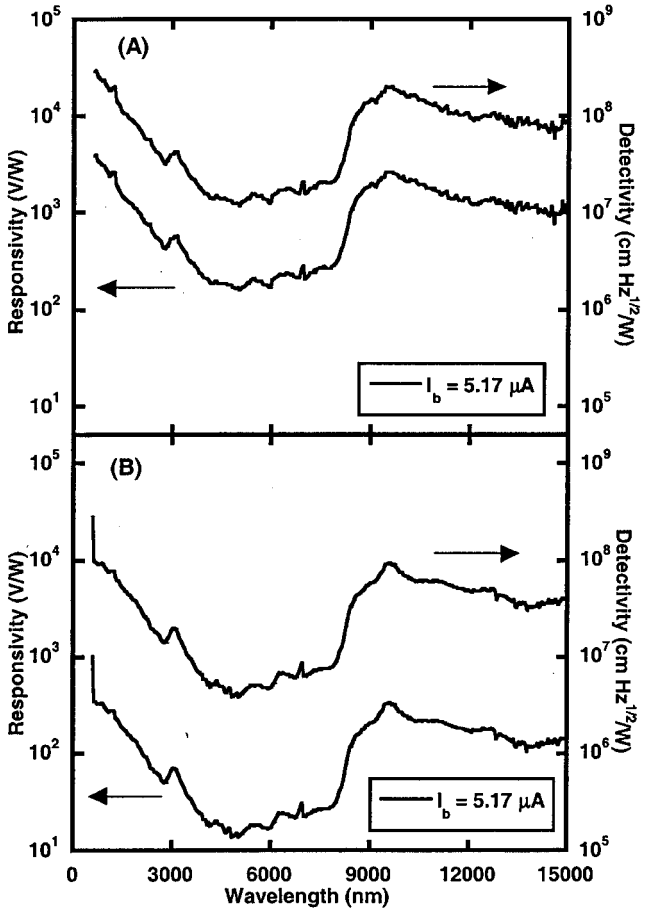

Fig. 8. Measured responsivities and detectivities as a function of wavelength for (a) 400 μm × 400 μm size and (b) 1.5 mm × 1.5 mm size (b) microbolometers.

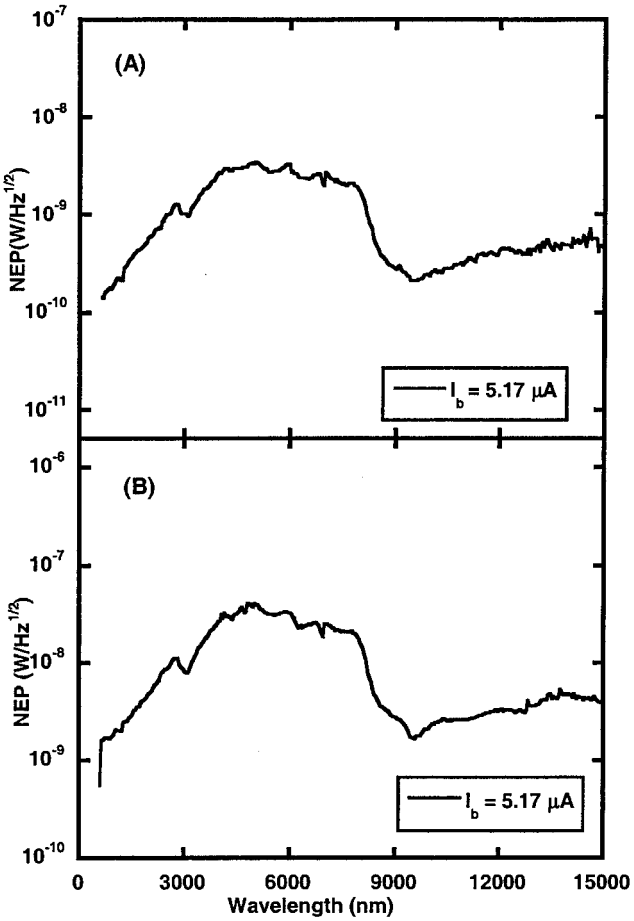

Fig. 9. Measured noise equivalent power as a function of wavelength for (a) 400 μm × 400 μm size and (b) 1.5 mm × 1.5 mm size microbolometers.

capacities C are 2.52×10^{-7} J/K and 1.47×10^{-6} J/K, respectively. The values for G/η were then calculated from the measured data to be 2.59×10^{-5} W/K and 1.12×10^{-4} W/K for the small area and large area devices. The absorptivities were extracted from the calculated G/η value and the measured G to be 60% for the small devices and 50% for the large devices. This represents a relatively strong IR absorption for the broadband YBaCuO thermometer, comparable to the predictions of the transmission line model used to design the structures. At this time, absorptivities were not verified by direct measurements. A

summary of the measured and extracted characteristics is presented in Table I.

V. Conclusion

Room-temperature broad-band microbolometers based on semiconducting YBaCuO were developed for far IR detection to be used for radiometric measurements at 30 Hz frame rate. The bolometers were micromachined on a 350-nm Si_3N_4 supporting membrane suspended approximately 6 μm above the substrate. A double-mirror structure was designed to achieve a relatively uniform spectral response up to 100 μm wavelength. The microbolometers exhibited a relatively strong absorptivity of $\sim$59% in the 0.6–15 μm wavelength band.

The 400 $\times$ 400 μm^2 1 $\times$ 4 microbolometer arrays displayed responsivities and detectivities of 1.56×10^3 V/W and 1.25×10^8 cm $Hz^{1/2}$/W, respectively, at a bias current of 4.65 μA. The large area single pixels (1.5 $\times$ 1.5 mm^2), on the other hand, had a responsivity of 158 V/W and a detectivity of 3.48×10^7 cm $Hz^{1/2}$/W at $I_b = 4.28$ μA. The measured noise equivalent power was 3.21×10^{-10} W/$Hz^{1/2}$ for small size arrays whereas, the large area single pixels showed NEP of 4.3×10^{-9} W/$Hz^{1/2}$. The power normalized $1/f$ noise corner frequency was less than or equal to 2 Hz/μW for large area detectors, while much smaller values, ($<$1 Hz/μW) were observed on small area detectors. These results are very promising for uncooled broadband microbolometer technology.

Acknowledgment

The authors would like to thank E. Kist of NASA Langley Research Center for the guidance he provided in this project and N. Amarasinghe for his help in packaging the devices.

References

[1] T. Breen, M. Kohin, C. A. Marshall, R. Murphy, T. White, A. L. Leary, and T. Parker, "Even more applications of uncooled microbolometer sensors," *SPIE*, vol. 3698, pp. 308–318, 1999.

[2] R. B. Lee, III, B. R. Barkstrom, H. C. Bitting, D. A. H. Cormmelynck, J. Paden, D. K. Pandey, K. J. Priestley, G. L. Smith, S. Thomas, K. L. Thornhill, and R. S. Wilson, "Prelaunch calibrations of the Clouds and the Earth's Radiant Energy System (CERES) tropical rainfall measuring mission and Earth Observing System Morning (EOS-AM1) spacecraft thermister bolometer sensors," *IEEE Trans. Geosci. Remote Sensing*, vol. 36, pp. 1173–1185, 1998.

[3] P. W. Kruse, "Principles of uncooled infrared focal plane arrays," in *Uncooled Infrared Imaging Arrays and Systems, Semiconductors and Semimetals*, P. W. Kruse and D. D. Skatrud, Eds. New York: Academic, 1997, vol. 47, pp. 17–42.

[4] A. Jahanzeb, C. M. Travers, Z. Çelik-Butler, D. P. Butler, and S. Tan, "A semiconductor YBaCuO microbolometer for room temperature IR imaging," *IEEE Trans. Electron Devices*, vol. 44, pp. 1795–1801, 1997.

[5] C. M. Travers, A. Jahanzeb, D. P. Butler, and Z. Çelik-Butler, "Fabrication of semiconducting YBaCuO surface micromachined bolometer arrays," *J. Microelectromech. Syst.*, vol. 6, pp. 271–276, 1997.

[6] J. Gray, Z. Çelik-Butler, D. P. Butler, and M. Almasri, "Semiconducting YBaCuO infrared detecting bolometers," *SPIE*, vol. 3436, pp. 555–565, 1998.

[7] J. Gray, Z. Çelik-Butler, and D. P. Butler, "MgO sacrificial layer for micromachining uncooled Y–Ba–Cu–O IR microbolometers on Si_3N_4 bridges," *J. Microelectromech. Syst.*, vol. 8, pp. 192–199, 1999.

[8] M. Almasri, D. P. Butler, and Z. Çelik-Butler, "Self-supporting infrared microbolometers with low-thermal mass," *J. Microelectromech. Syst.*, vol. 10, pp. 469–476, 2001.

[9] ——, "Semiconducting YBCO bolometers for uncooled IR detection," *SPIE*, vol. 4028, pp. 17–26, 2000.

[10] D. P. Butler, Z. Çelik-Butler, and R. Sobolewski, "Yttrium barium copper oxide as an infrared radiation sensing material," in *Handbook of Advanced Electronic and Photonic Materials and Devices*, H. S. Nalwa, Ed., 2001, vol. 3, pp. 169–195.

[11] T. H. Kim, M. S. Han, M. S. Jeoung, J. H. Kwon, N. S. Yim, G. S. Lee, E. T. Kim, S. R. Hahn, H. C. Kwon, Y. Bin, Y. T. Jeoung, and J. M. Kim, "Single element photoconductive $Hg_{0.79}Cd_{0.21}Te$ IR detector fabrications and their characteristic," *SPIE*, vol. 3436, pp. 91–97, 1998.

[12] A. Manissadjian, P. Costa, P. Tribolet, and G. Destefanis, "HgCdTe performance for high operating temperatures," *SPIE*, vol. 3436, pp. 150–161, 1998.

[13] D. P. Osterman, R. Patt, R. Hunt, K. Lane, and S. Gaalema, "Uncooled micromachined themopile arrays and read-out circuits," *SPIE*, vol. 3698, pp. 376–386, 1999.

[14] J. M. Gildemeister, A. T. Lee, and P. L. Richards, "Monolithic arrays of absorber-coupled voltage-biased superconducting bolometers," *Appl. Phys. Lett.*, vol. 77, pp. 4040–4042, 2000.

[15] M. J. M. E. de Nivelle, M. P. Bruijin, R. de Vries, J. J. Wijnbergen, P. A. J. de Korte, S. Sanchez, M. Elwenspoek, T. Heidenblut, B. Schwierzi, W. Michalke, and E. Steinbeiss, "Low noise high T_c-superconducting bolometers on silicon nitride membranes for far-infrared detection," *J. Appl. Phys.*, vol. 82, pp. 4719–4726, 1997.

[16] S. Sanchez, M. Elwenspoek, C. Gui, M. J. M. E. de Nivelle, R. de Vries, P. A. J. de Korte, M. P. Bruijin, J. J. Wijnbergen, W. Michalke, E. Steinbeiss, T. Heidenblut, and B. Schwierzi, "A high-Tc superconductor bolometer on a silicon nitride membrane," *J. Microelectromech. Syst.*, vol. 7, pp. 62–68, 1998.

[17] B. R. Johnson, T. Ohnstein, C. J. Han, R. Higashi, P. W. Kruse, R. A. Wood, H. March, and S. B. Dunham, "$YBa_2Cu_3O_7$ superconducting microbolometer arrays rabricated by silicon micromachining," *IEEE Trans. Appl. Superconduct.*, vol. 3, pp. 2856–2859, 1993.

[18] Z. Mai, X. Yi, X. Zhao, F. Zhao, and L. Liu, "High Tc superconducting microbolometer detector arrays," *SPIE*, vol. 2894, pp. 163–169, 1996.

[19] V. N. Leonov, "Capabilities of antenna-coupled superconducting microbolometers," *J. Phys. IV France*, vol. 8, pp. 267–270, 1998.

[20] A. Gauge, E. Caristan, D. Robbes, C. Gunther, A. Stentz, and A. Kreisler, "Submillimeter wave detection with high temperature superconducting bolometers," *J. Phys. IV France*, vol. 8, pp. 263–266, 1998.

[21] Y. Karehi, T. Yotsuya, T. Kusaka, Y. Suzuki, S. Ogawa, and H. Imokawa, "Infrared radiation detector with $YBa_2Cu_3O_x$ thin film," *J. Appl. Phys.*, vol. 37, pp. 4774–4781, 1998.

[22] E. L. Dereniak and G. D. Boreman, *Infrared Detectors and Systems*. New York: Wiley, 1996, pp. 395–438.

[23] G. Yu and A. J. Heeger, "Photoinduced charge carriers in insulating cuprates: Fermi glass insulator, metal-insulator transition and superconductivity," *Int. J. Modern Phys. B*, vol. 7, p. 3751, 1993.

[24] C. Marshall, N. Butler, R. Blackwell, R. Murphy, and T. Breen, "Uncooled infrared sensor with digital focal plane array," *SPIE*, vol. 2746, p. 23, 1996.

[25] B. I. Craig, R. J. Watson, and M. H. Unewisse, "Anisotropic excess noise within a Si : H," *Solid-State Electron.*, vol. 39, p. 807, 1996.

[26] P. W. Kruse, "A comparison of the limits to the performance of thermal and photon detector imaging arrays," *Infrared Phys. Technol.*, vol. 36, pp. 869–882, 1995.

Mahmoud Almasri (S'01) received the B.Sc. and M.Sc. degrees in physics from Bogazici University, Istanbul, Turkey, in 1995 and 1997, respectively, and the Ph.D. degree in electrical engineering from Southern Methodist University (SMU), Dallas, TX, in 2001.

He is currently working as a research scientist at General Monitors laboratories, Lake Forest, CA. His graduate research was on developing broadband and far-infrared detectors for thermal imaging, night vision and space applications. He coauthored 12 conference and journal papers in these areas.

Dr. Almasri was awarded the Southern Methodist University, "Frederick E. Terman Award," in electrical engineering in 1999–2000, and the Southern Methodist University "Graduate Student Research Award," Jointly Sponsored by SMU Chapter of Sigma Xi and Office of Research and Graduate Studies at the annual Research Day in 2001. He is a Student Member of SPIE.

Zeynep Çelik-Butler (S'84–M'87–SM'98) received dual B.S. degrees in electrical engineering and physics from Bogaziçi University, Istanbul, Turkey, in 1982. She received the M.S. and Ph.D. degrees in electrical engineering in 1984 and 1987, respectively, from the University of Rochester, NY.

From 1983 to 1984, she was an IBM Predoctoral Fellow and from 1985 to 1987, she was an Eastman Kodak Predoctoral Fellow. She joined the Department of Electrical Engineering at Southern Methodist University (SMU), Dallas, TX, in 1987 as an Assistant Professor; was tenured and promoted to Associate Professor in 1993. She was the holder of J. Lindsay Embrey Trustee Assistant Professorship from 1990 to 1993. She served as the Assistant Dean of Graduate Studies and Research from 1996 to 1999. She is currently a Professor of Electrical Engineering. She served in various technical committees including 1988, 1989 IEEE-IEDMs and Annual Symposia on Electronic Materials, Processing and Characterization (1989–1992) and International Conference on Noise in Physical Systems and $1/f$ Fluctuations (1993, 1999, and 2001). Her research interests include microelectromechanical systems, infrared detectors, noise in semiconductor and superconductor devices, and high T_c-superconductivity. She has four patents, four book chapters, and over 100 journal and conference publications in these fields.

Dr. Çelik-Butler is a Senior Member of IEEE, member of Eta Kappa Nu, and the American Physical Society (APS). She is a Distinguished Lecturer for the IEEE-Electron Devices Society. She was the General Chair of TEXMEMS II Workshop. She is currently the technical editor for Fluctuation and Noise Letters. She has received several awards including the IEEE-Dallas Section Electron Devices Society Outstanding Service Awards (1995 and 1997), IEEE-Electron Devices Society, Service Recognition Award (1995), Outstanding Electrical Engineering Graduate Faculty Awards (1996, 1997, and 2001), and Southern Methodist University Sigma Xi Research Award (1997).

Donald P. Butler (S'81–M'85–SM'98) received the B.A.Sc. degree in engineering science: physics option from the University of Toronto, Toronto, ON, Canada, in 1980 and the M.S. and Ph.D. degrees in electrical engineering from the University of Rochester, NY, in 1981 and 1986, respectively.

He performed his graduate research at the Laboratory for Laser Energetics investigating the nonequilibrium behavior of superconductor thin films in response to picosecond electrical and optical excitations. He continued his graduate research as a Research Associate in 1986. In 1987, he joined the Electrical Engineering Department at Southern Methodist University (SMU), Dallas, TX, as an Assistant Professor. In 1993, he was promoted to the rank of Associate Professor and Professor in 2001. At SMU, his research has included the optical control of superconductive microwave transmission line filters, the investigation of high-temperature superconductors for hybrid superconductor–semiconductor electronics, the application of high-temperature superconductors to microwave mixing and parametric conversion, the characterization of GaAs MMICs at cryogenic temperatures, and uncooled infrared detectors. His current research is focused on uncooled infrared detection, microelectromechanical devices (MEMS), pulsed laser deposition, and annealing of thin films. He pioneered the application of semiconducting YBaCuO to uncooled infrared detection. He has published more than 60 journal articles and conference presentations and holds four patents.

Dr. Butler is a Member of the SPIE and the American Physical Society (APS) and is active in the IEEE. For the past 10 years, he has served in various positions for the IEEE at the chapter, section, and international level. He is a recipient of the IEEE Third Millennium Medal. He is an Electron Device Society Distinguished Lecturer. He is currently Chair of the IEEE Dallas Section.

Alparslan Yaradanakul (S'01) received the B.S. and M.S. degrees in physics with emphasis in optoelectronics from Bogazici University, Istanbul, Turkey, in 1994 and 1996, respectively. He is pursuing the Ph.D. degree in electrical engineering from Southern Methodist University (SMU), Dallas, TX, and currently working as a Research Engineer in mechanical engineering department of Texas A&M University, College Station.

His research interests include fabrication and characterization of infrared detectors on silicon and flexible substrates, optical characterization of materials using fiber-optic technique and optoelectronics. He has coauthored four journal papers and eight conference publications in these areas.

Mr. Yaradanakul has received a few awards, including SMU Outstanding Graduate Student Award, 2001 and Graduate Study Abroad Scholarship from Turkish Ministry of Education, 1998. He is a Student Member of the American Physical Society (APS).

Ali Yildiz received the B.Sc. and M.Sc. degrees in physics from Bogazici University, Turkey, in 1996 and 1998, respectively. He is currently a graduate student at Southern Methodist University (SMU), Dallas, TX working toward the Ph.D. degree in electrical engineering.

His research area includes uncooled infrared bolometric and pyroelectric detectors, including modeling, material analysis, fabrication, electrical and optical characterization, and implementation of room temperature infrared detectors on flexible substrates.